OPEN

NPG Asia Materials (2016) 8, e244; doi:10.1038/am.2016.16
www.nature.com/am

ORIGINAL ARTICLE

Trimodally porous SnO_2 nanospheres with three-dimensional interconnectivity and size tunability: a one-pot synthetic route and potential application as an extremely sensitive ethanol detector

Ji-Wook Yoon[1,3], Seung Ho Choi[1,3], Jun-Sik Kim[1], Ho Won Jang[2], Yun Chan Kang[1] and Jong-Heun Lee[1]

The rapid and effective transfer of chemical reactants to solid surfaces through porous structures is essential for enhancing the performance of nanomaterials for various energy and environmental applications. In this paper, we report a facile one-pot spray pyrolysis method for preparing highly reactant-accessible and porous SnO_2 spheres, which have three-dimensionally interconnected and size-tunable trimodal (microscale, mesoscale and macroscale) pores. For this synthetic method, macroscale polystyrene spheres and mesoscale-diameter, long carbon nanotubes were used as sacrificial templates. The promising potential of the SnO_2 spheres with trimodal pores (sizes ≈3, 20 and 100 nm) was demonstrated by the unprecedentedly high response to several p.p.b. levels of ethanol. Such an ultrahigh response to ethanol is explained with respect to the hierarchical porosity and pore-size-dependent gas diffusion mechanism.
NPG Asia Materials (2016) **8,** e244; doi:10.1038/am.2016.16; published online 11 March 2016

INTRODUCTION

Nanoparticles with a high surface area-to-volume ratio offer many distinct advantages, such as a high chemical reactivity at the surface of the particles, unique near-surface electrical properties and the rapid diffusion of reactants into the solid lattice, that provide new and enhanced functionalities for catalysts, gas sensors, semiconductors and Li-ion batteries.[1–4] However, most nanoparticles tend to aggregate into large and dense secondary agglomerates because of the strong van der Waals attractions between the particles, which hamper mass transfer to the inner part of agglomerates. This in turn considerably affects the performance of such materials in the aforementioned applications. Porous solids consisting of, or assembled from, nanostructures are excellent nanoarchitectures that can significantly enhance the mass transfer of chemical reactants (for example, gases or ions) to reaction surfaces with minimal sacrifice of the active surfaces in the nanostructures. In general, the reactants diffuse towards the reactive surfaces via macropores, mesopores and micropores, and mass transfer through porous structures depends upon the pore size. For instance, different gas diffusion mechanisms, such as normal, Knudsen and surface diffusion, are predominant in macropores, mesopores and micropores, respectively. Therefore, to take best advantage of the benefits of porous nanostructures for energy and environmental applications involving surface/interface reactions, multimodal porous structures that contain macropores, mesopores and micropores are considered a promising platform. For this, the size, volume, distribution and interconnectivity of the different pores should be controlled precisely and independently.

Ordered mesoporous oxide nanostructures with highly connected, periodic and monodisperse pores are a good candidate for gas sensors, which are generally prepared by replicating ordered, mesoporous, silica templates.[5–11] However, such mesopores are typically smaller than 10 nm,[8–12] and it is difficult to create and control multimodal pores. Hierarchical porous and hollow oxide nanostructures, which are prepared through the solvothermal/hydrothermal self-assembly reactions of nanoscale building blocks, are also considered a reactant-accessible material platform.[13–19] However, because of the relatively low level of control over the self-assembly reactions, it is difficult to tune the size, volume and interconnectivity of the macropores, mesopores and micropores, which hampers any attempts to precisely design porous structures for the effective and rapid transport of reactants to the entire surface of such nanostructures.

In this study, highly reactant-accessible SnO_2 spheres with three-dimensionally interconnected, size-tunable, trimodal pores were prepared for the first time with a facile, one-pot, spray pyrolysis method. The promising potential of the trimodally porous SnO_2 (hereafter referred to as '3M-SnO_2') spheres as a chemiresistive-sensing material was demonstrated by their ultrahigh response to gases, even for p.p.b. level of ethanol.

[1]Department of Materials Science and Engineering, Korea University, Seoul, Republic of Korea and [2]Department of Materials Science and Engineering, Research Institute for Advanced Materials, Seoul National University, Seoul, Republic of Korea
[3]These authors contributed equally to this work.
Correspondence: Professor YC Kang or Professor J-H Lee, Department of Materials Science and Engineering, Korea University, Seoul 136-714, Republic of Korea.
E-mail: yckang@korea.ac.kr or jongheun@korea.ac.kr
Revised 25 September 2015; revised 11 December 2015; accepted 3 January 2016

EXPERIMENTAL PROCEDURES

Preparation of precursor materials

Polystyrene (PS) spheres (mean diameter ≈100 nm) were prepared with an emulsion-free polymerization method (Supplementary Figure S1a). In brief, styrene (30.0 ml, Sigma-Aldrich, St Louis, MO, USA), poly(sodium 4-styrenesulfonic acid) (0.25 g, Sigma-Aldrich) and sodium bicarbonate (0.15 g, $NaHCO_3$, 99.995%, Sigma-Aldrich) were dissolved in distilled water (300 ml), and the solution was stirred at 70 °C for 1 h. Potassium persulfate (0.15 g, $K_2S_2O_8$, 99.99%, Sigma-Aldrich) was then added to the solution, and it was vigorously stirred with a fluid mixer (300 r.p.m.) at 70 °C for 18 h under a N_2 atmosphere. Commercially available multi-walled carbon nanotubes (MWCNTs, diameter ≈20 nm) were purchased from Shenzhen Nanotech Port (Shenzhen, China) (Supplementary Figure S1b) and surface-modified with a 1:3 vol.% mixture of HNO_3 (0.15 g, 70%, Sigma-Aldrich) and H_2SO_4 (0.15 g, 95%, Sigma-Aldrich) at 80 °C. The resulting product was sequentially washed with distilled water and ethanol five times and then re-dispersed in distilled water (1 mg ml^{-1}).

Preparation of gas-sensing materials

The D-, 2M- and 3M-SnO_2 spheres were obtained via the spray pyrolysis of an aqueous solution, and the subsequent heat treatment of the precursor powders. A spray solution for the 3M-SnO_2 spheres was prepared by dissolving 1.7 g of tin(II) oxalate (SnC_2O_4, 98%, Sigma-Aldrich) in 250 ml of distilled water containing the well-dispersed surface-modified MWCNTs (1 mg ml^{-1}) and PS spheres (3.0 g). An appropriate volume of a hydrogen peroxide solution (30%, H_2O_2, Sigma-Aldrich) was added to the spray solution to stabilize the PS before dissolving the SnC_2O_4. The spray solution for the 2M-SnO_2 spheres was prepared without the surface-modified MWCNTs, while that for the D-SnO_2 spheres was prepared without both the surface-modified MWCNTs and PS spheres. The droplets of the spray solutions were generated with five ultrasonic transducers (resonant frequency = 1.7 MHz), which were subsequently transported to a high-temperature tubular reactor (700 °C, length = 1200 mm, diameter = 50 mm) by a flow of Ar gas (flow rate = 5 l min^{-1}). The retention time of the droplets in the high-temperature region was approximately 15 s. The as-prepared precursor powders were collected in a Teflon bag filter (Clean & Green-tech, Seoul, Korea) in the particle-collecting chamber. A detailed schematic of the experimental setup used for the spray pyrolysis is shown in Supplementary Figure S2. The three precursor powders were converted into the D-, 2M- and 3M-SnO_2 spheres via a heat treatment at 600 °C for 3 h in air. The heating rate was 10 °C min^{-1}.

Characterization

The morphology of the prepared materials was observed with scanning electron microscopy (S-4800, Hitachi, Tokyo, Japan) and high-resolution transmission electron microscopy (HR-TEM, FEI Technai 20, FEI, Hillsboro, OR, USA). The crystal structure of the prepared materials was investigated with powder X-ray diffraction (X'Pert PRO MPD, Philips, Amsterdam, Netherlands) using CuKα radiation ($\lambda = 1.5418$ Å). The specific surface area of the various gas-sensing materials was calculated from Brunauer–Emmett–Teller (BET) analysis of the N_2 adsorption measurements (TriStar 3000, Micromeritrics, Norcross, MN, USA).

Characterization of the gas-sensing properties

The powders were dispersed in distilled water and alumina substrates (size = 1.5 × 1.5 mm^2), which had two Au electrodes on the top surface and a microheater on the bottom surface, were drop-coated with the slurry. Prior to the measurements, the sensor was heated at a power of 570 mW (550 °C) for 2 h to remove any hydroxyl content and stabilize the sensor. The sensor was contained within a specially designed quartz tube (1.5 cm^3), and a constant flow (flow rate = 500 cm^3 min^{-1}) of air and analyte gas was switched with a four-way valve to change the atmosphere. The two-probe DC resistance of the sensor was measured with an electrometer connected to a computer. The responses of the sensors to 5 p.p.m. of ethanol, formaldehyde, ammonia, carbon monoxide, hydrogen, benzene, toluene and xylene at 350 − 450 °C were calculated with the formula $R_a R_g^{-1}$, where R_a is the resistance in air and R_g is the resistance in the analyte gas.

RESULTS AND DISCUSSION

Formation of trimodally porous SnO_2 spheres

Aqueous droplets containing tin (II) oxalate, PS spheres (diameter ≈100 nm; Supplementary Figure S1a) and MWCNTs (diameter ≈20 nm; Supplementary Figure S1b) were generated with an ultrasonic evaporator (Scheme 1a). These aqueous droplets were then converted into SnO_2/MWCNTs composite spheres with spherical macropores by performing spray pyrolysis at 700 °C (Scheme 1b). The MWCNTs and a small amount of the residual PS were completely decomposed by subjecting the composite spheres to a heat treatment (600 °C for 3 h; Scheme 1c), which in turn formed the trimodal pores: (i) macroscale (approximately 100 nm) spherical pores, (ii) elongated and connected mesoscale diameter (approximately 20 nm) pores, and (iii) microscale and mesoscale (approximately 3 nm) pores created by the outgassing of gases evolved during the decomposition of the carbon-based precursors (smallest pores in Scheme 1c). For comparison purposes, bimodally porous SnO_2 (2M-SnO_2; pore sizes ≈3 and 100 nm) spheres and dense SnO_2 (D-SnO_2) spheres were also prepared via the spray pyrolysis of MWCNT-free precursor droplets with and without the spherical PS templates, respectively.

Structural and morphological properties

All three of the as-prepared precursor spheres for the D-, 2M- and 3M-SnO_2 spheres were composed of a tetragonal SnO_2 phase (JCPDS no. 41–1445) (Supplementary Figure S3). The higher crystallinity of PS-mediated macroporous precursor spheres can be explained by thermal promotion of SnO_2 crystallization owing to excess heat generated by the combustion of PS. The weight loss (%) caused by the decomposition of the precursor powders was investigated with thermogravimetric analysis (TGA, heating rate = 20 °C min^{-1}; air atmosphere; Supplementary Figure S4). Even though the three types of precursor spheres had been heat-treated at a high pyrolysis temperature of 700 °C, a total weight loss of up to 18% was observed as the TGA temperature increased to 700 °C. This is because the

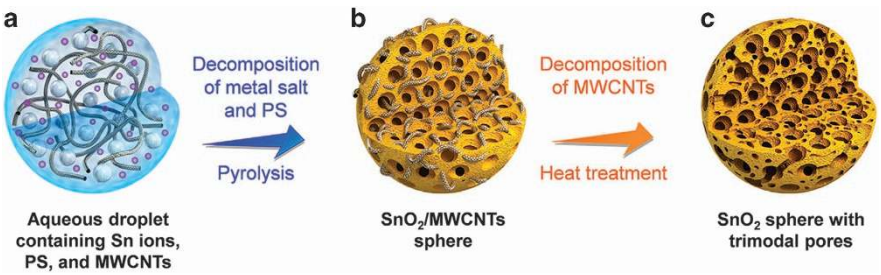

Scheme 1 Scheme illustrating the formation of SnO_2 nanospheres with trimodal porosity. (**a**) Aqueous droplets of spray solution, (**b**) as-prepared precursor spheres after spray pyrolysis, and (**c**) SnO_2 spheres with trimodal pores (3M-SnO_2) after heat treatment at 600 °C for 3 h.

retention time of the spray pyrolysis (approximately 15 s) is probably insufficient to complete the decomposition reactions. Comparing the TGA curves of the precursors for the 2M- and 3M-SnO_2 clearly indicates that the weight loss between 200 and 400 °C is due to the decomposition of the residual PS, and thus the weight loss between 400 and 600 °C can be attributed to the decomposition of MWCNTs. The TGA curves indicate that most of the PS decomposes during the spray pyrolysis reaction, and the MWCNTs and a small amount of the residual PS can be completely removed by performing the heat treatment at approximately 600 °C.

The precursors for the D-SnO_2 exhibit a clean surface with a dense inner structure (Supplementary Figures S5a and d). In contrast, the precursors for the 2M- (Supplementary Figures S5b and e) and 3M-SnO_2 spheres (Supplementary Figures S5c and f) exhibit macroporous inner structures with spherical pores (size ≈100 nm), indicating the successful decomposition of the sacrificial PS templates. In addition, it is clear that the MWCNTs are still present in the precursor spheres after the spray pyrolysis (Supplementary Figures S5c and f). The MWCNTs were well dispersed within the spheres, which was confirmed by the cross-sectional TEM image of the sphere prepared by focused ion-beam treatment (Supplementary Figure S6).

The D-, 2M- and 3M-SnO_2 spheres were prepared via the heat treatment at 600 °C for 3 h. The average crystallite sizes of the D-, 2M- and 3M-SnO_2 determined from (110), (101) and (211) peaks by Sherrer's equation are 6.29, 8.59 and 8.95 nm, respectively, after the heat treatment (Supplementary Figure S7). The scanning electron microscopic and HR-TEM images of the D-SnO_2 after the heat treatment (Figures 1a, d and g) show that spheres with a clean surface and dense

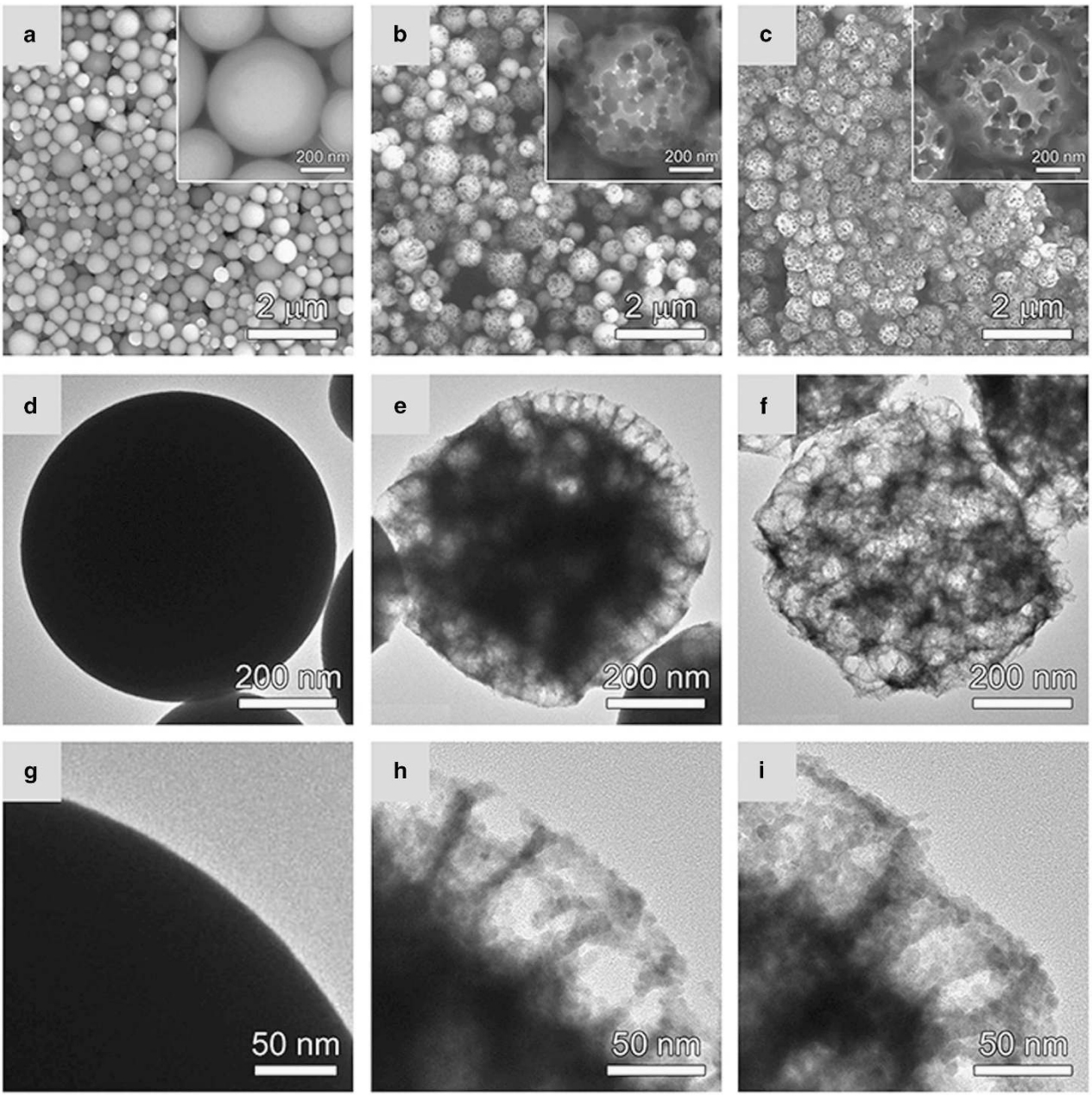

Figure 1 (**a**–**c**) Scanning electron microscopy and (**d**–**i**) high-resolution transmission electron microscopy images of the (**a**, **d**, **g**) dense SnO_2 spheres (D-SnO_2), (**b**, **e**, **h**) SnO_2 spheres with bimodal pores (2M-SnO_2) and (**c**, **f**, **i**) SnO_2 spheres with trimodal pores (3M-SnO_2).

inner structure were obtained. On the other hand, both the 2M- and 3M-SnO_2 have many craters in their surfaces (Figures 1b and c) and a macroporous inner structure (Figures 1e, f, h and i), which was formed by the PS templates. The similar inner morphologies of the as-prepared precursors and heat-treated 2M- and 3M-SnO_2 show that most of the PS templates decomposed during the spray pyrolysis. In addition, the 3M-SnO_2 (Figure 1f) have brighter contours in the inner structure than their precursors (Supplementary Figure S5c), as well as that of the 2M-SnO_2 (Figure 1e). Furthermore, after a thorough HR-TEM analysis, no MWCNTs were observed in the 3M-SnO_2, indicating a further enhancement of the overall porosity because of the complete decomposition of the MWCNTs.

Pore-size distribution and surface area analysis

The N_2 adsorption/desorption isotherms of the 2M- and 3M-SnO_2 have a shape that is between a type II and type IV isotherm with H3 hysteresis loops, indicating the presence of mesopores, whereas the isotherm of the D-SnO_2 has the form of a type II isotherm, which is typical for non-porous structures (Figure 2a). The pore-size distribution and specific surface area of the three different SnO_2 spheres were derived from the Barrett–Joyner–Halenda and the BET methods, respectively. The BET surface area of the 3M-SnO_2 spheres was determined to be 53.2 $m^2 g^{-1}$ (Figure 2b), which is significantly higher than those of the 2M- (18.4 $m^2 g^{-1}$; Figure 2c) and D-SnO_2 spheres (2.42 $m^2 g^{-1}$; Figure 2d). Pores with a mean diameter of approximately 3 nm were found in both the 2M- (Figure 2f) and 3M-SnO_2 spheres (Figure 2e), which are attributed to the outgassing produced by the decomposition of the PS templates. On the other hand, pores with diameters of approximately 20 nm were only observed in the 3M-SnO_2 spheres (Figure 2e), which were formed by the combustion of the sacrificial MWCNT templates that had the same diameter. These results are consistent with the HR-TEM observations. No significant pores were observed in the D-SnO_2 spheres (Figure 2g). It was difficult to determine the size of the macroscale pores (approximately 100 nm) with BET analysis. However, in association with the scanning electron microscopic and HR-TEM analyses in Figure 1, we can safely say that the 3M-SnO_2 spheres have three different sizes (approximately 3, 20 and 100 nm) of pores, whereas the 2M-SnO_2 spheres only exhibit two different sizes (approximately 3 and 100 nm).

Gas-sensing characteristics

To investigate the effects of multimodal porosity on the gas accessibility of the nanoparticles, the ethanol-sensing characteristics of the D-, 2M- and 3M-SnO_2 spheres were measured between 350 and 450 °C (Figure 3). The three sensors all exhibit typical n-type sensing behaviors in which the sensor resistance decreases when exposed to a reducing gas (ethanol) and returns to the original resistance in an air atmosphere (Supplementary Figure S8). The D-SnO_2 spheres exhibit the lowest response ($S = R_a R_g^{-1}$, where R_a and R_g are the resistances in air and the analyte gas, respectively) and relatively slow response and recovery kinetics (Figure 3a). The maximum response to 5 p.p.m. of ethanol is 34.2 at 450 °C and the times taken to reach a 90% variation in the resistance upon exposure to ethanol and air (τ_{res} and τ_{recov}, respectively) are 6 and 1485 s, respectively. The maximum ethanol response of the 2M-SnO_2 spheres (117.6) occurs at 350 °C, which is 3.4 times higher than that of the D-SnO_2 spheres. In addition, the τ_{res} and τ_{recov} values have significantly decreased to 2 and 550 s, respectively (Figure 3b). This indicates that the introduction of macropores (approximately 100 nm) and mesopores (approximately 3 nm) within spheres via the sacrificial PS templates is an effective method for enhancing both the gas response and response/recovery speeds. The 3M-SnO_2-based sensor (Figure 3c) exhibits an ultrahigh gas response of 316.5 at 400 °C, as well as fast τ_{res} and τ_{recov} values of 1 and 416 s, respectively, showing a further enhancement of the gas-sensing properties.

In general, the gas responses of n-type oxide semiconductors to a reducing gas as a function of sensing temperature show bell-shape curve because the surface reaction between analyte gas and adsorbed oxygen is difficult at very low sensing temperature, whereas, at excessively high sensing temperature, the analyte gas is consumed by the oxidation at the inactive upper part of sensing film (or outer part

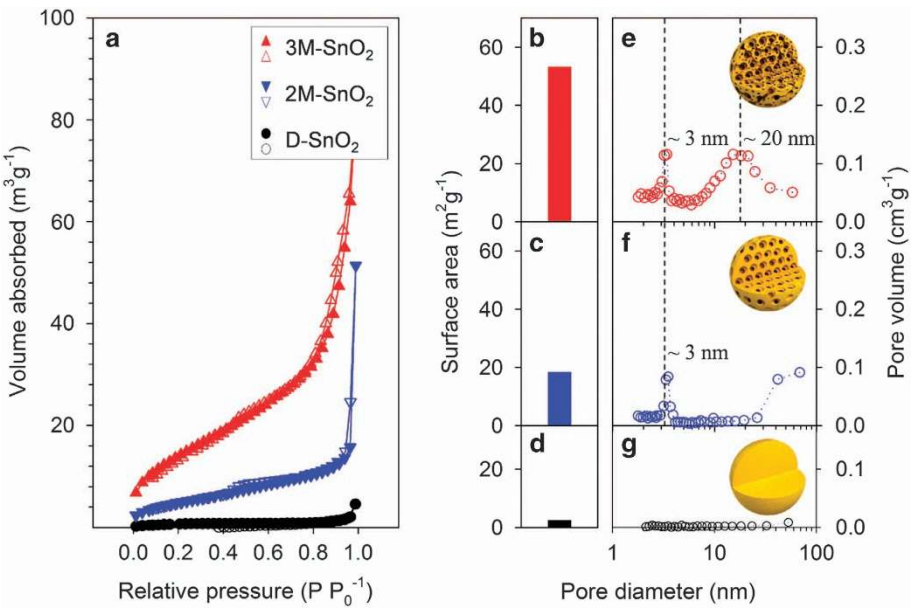

Figure 2 (**a**) N_2 adsorption/desorption isotherms of the 3M- (red), 2M- (blue) and D-SnO_2 (black). (**b**–**g**) The corresponding BET surface areas and pore-size distributions of the (**b**, **e**) 3M-, (**c**, **f**) 2M- and (**d**, **g**) D-SnO_2.

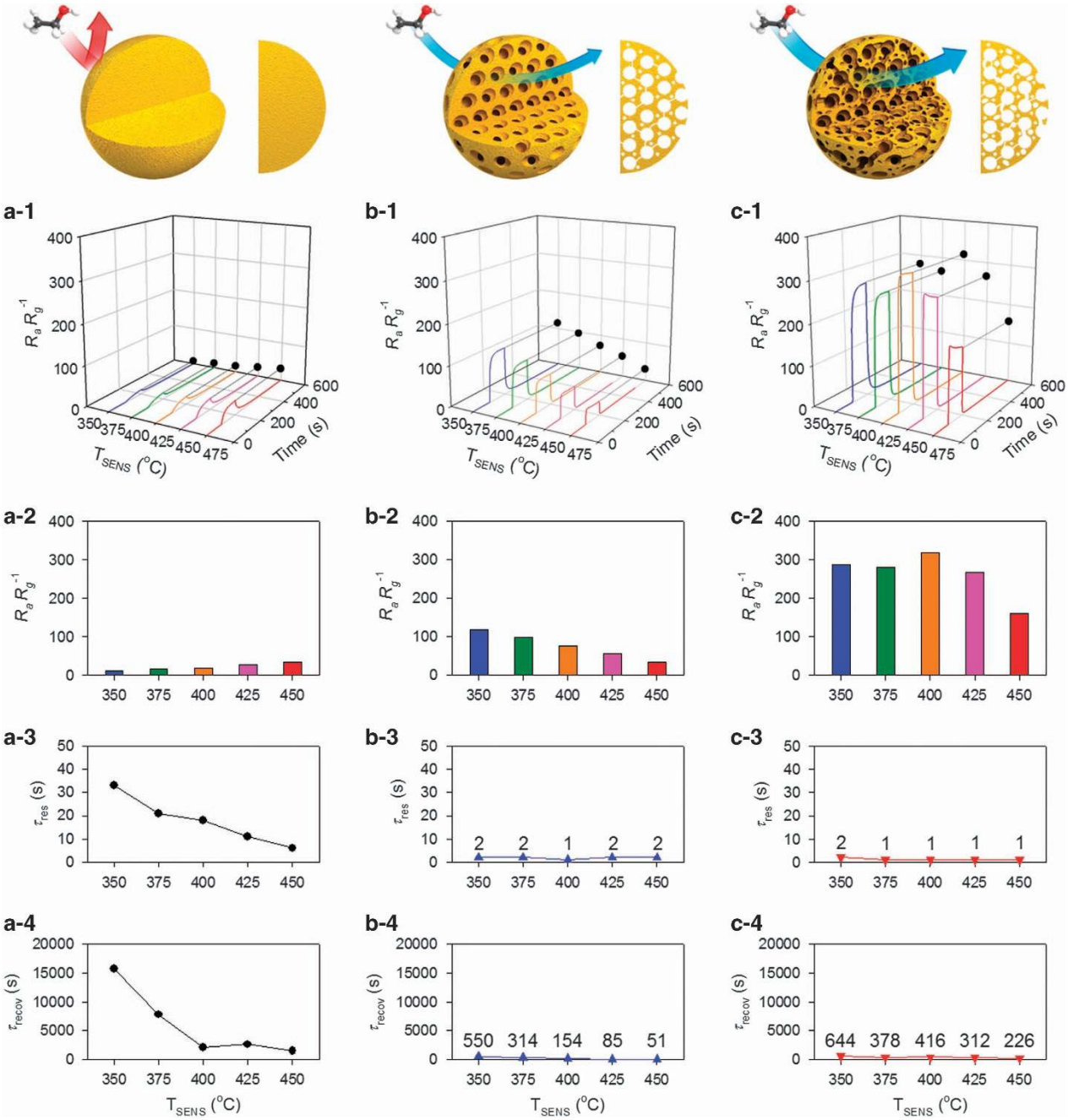

Figure 3 Gas-sensing characteristics of the (**a**) D-, (**b**) 2M- and (**c**) 3M-SnO_2 spheres to 5 p.p.m. of ethanol. (**a**-1, **b**-1, **c**-1) The gas response (R_a R_g^{-1}) transients as functions of time and sensing temperature. (**a**-2, **b**-2, **c**-2) The gas response and the (**a**-3, **b**-3, **c**-3) 90% response time (τ_{res}) and (**a**-4, **b**-4, **c**-4) 90% recovery time (τ_{recov}) of the three sensors.

of porous spheres in the present study) before the sensing reaction. Thus, when the larger amount of analyte gas is provided by the effective gas diffusion through the well-defined pores, the higher sensing temperature would be necessary to counteract the sensing reaction via the oxidative consumption of analyte gas, which leads to the increase of temperature for maximum gas response (T_M). This is analogous to the analysis by Sakai *et al.*[20] that the T_M value increases with decreasing film thickness. The T_M value in 3M-SnO_2 sensors (400 °C) higher than that in 2M-SnO_2 spheres (~350 °C) can be understood in this perspective although further study is required to understand temperature dependence of gas response in D-SnO_2-based sensor.

The gas responses (158.8 – 316.5) of the 3M-SnO_2-based sensor over 350 – 450 °C are significantly higher than the maximum gas response of the 2M-SnO_2-based sensor (117.6), which is evidence that the size and distribution of the mesopores are key parameters in determining the gas response. Li *et al.*[21] reported that the gas responses of mesoporous SnO_2-based sensors to hydrogen and carbon monoxide increase as the size of the pores increase from 1 to 10 nm. Vuong *et al.*[22] also reported that the hydrogen response of nanocrystalline SnO_2 thin

films increases as the mesopore size increases. Thus the pore size is an important parameter for the diffusion of gas through mesoporous structures. For mesopores ranging from 2 to 50 nm in size, Knudsen diffusion, which accounts for collisions between the pore walls and gas molecules, is known to be predominant.[20] The Knudsen diffusion coefficient (D_K) is defined as $(4r/3)(2RT/\pi M)^{1/2}$, where r, R, T and M are the pore radius, ideal gas constant, temperature and molecular weight of the diffusing gas, respectively. Thus D_K is proportional to the pore size when the same gas and sensing temperature are used. Accordingly, the introduction of MWCNT-assisted, large mesopores (approximately 20 nm in size) in addition to the small mesopores (approximately 3 nm in size) significantly increases the diffusion of an analyte gas to the inner regions of the porous SnO_2 spheres. Moreover, the elongated morphology of the MWCNT templates has a key role in enhancing the interconnectivity between the macropores (approximately 100 nm in size) and small mesopores. This is supported by the increase in the surface area from 18.4 (2M-SnO_2 spheres) to 53.2 $m^2 g^{-1}$ (3M-SnO_2 spheres). However, porous SnO_2 spheres prepared only by MWCNT templates without PS balls showed relatively low responses ($R_a R_g^{-1} = 18.3–34.3$) to 5 p.p.m. ethanol at 350–450 °C (Supplementary Figure S9), indicating that one-dimensional mesoporosity is insufficient to achieve giant chemiresistivity. Therefore, the ultrahigh response of the 3M-SnO_2-based sensor to 5 p.p.m. of ethanol at 400 °C (316.5) and fast response (1 s) can be attributed to the enhanced gas accessibility of the porous spheres with three-dimensionally interconnected trimodal pores and increased Knudsen diffusion through the relatively large mesopores.

The highest response of the 3M-SnO_2-based sensor to 5 p.p.m. of ethanol is 316.5 at 400 °C, which is one of the highest values ever reported in the literature for undoped SnO_2-based gas sensors (Figure 4 and Supplementary Table S1).[23–36] The 3M-SnO_2-based sensor exhibits a high response (28.1) to even 0.25 p.p.m. of ethanol (Figure 5). The detection limit of the sensor was calculated to be 4.9 p.p.b. when $R_a R_g^{-1} > 1.2$ was used as the criterion for gas sensing. The sensor showed highly stable response to 5 p.p.m. ethanol at 400 °C for 30 days (Supplementary Figure S10). In addition, for all sensing temperatures, the 3M-SnO_2-based sensor exhibits a high selectivity for ethanol, with low cross-responses to other interference gases, such as formaldehyde, ammonia, carbon monoxide, hydrogen, benzene, toluene and xylene (Supplementary Figure S11). The selective detection of ethanol in SnO_2 gas sensor is well known,[37] which can be explained by high catalytic activity of SnO_2 for ethanol oxidation[38] as well as high reactivity of ethanol compared with other gases, such as aldehydes, aromatics and ketones.[39] This offers excellent gas-sensing characteristics for monitoring drunk driving. To screen an intoxicated driver, the selective detection of 200 p.p.m. of ethanol is sufficient for a direct-breath measurement.[36] Recent progress in this field suggests that the detection of sub-p.p.m. level of ethanol, which are exhaled by drunk drivers and then diluted with the air in the automotive cabin a few seconds after closing the car door, could be used for the unobtrusive monitoring of drunk driving without the need for time-consuming breath sampling.[40] The 3M-SnO_2-based sensor with ultrahigh, rapid and stable response to p.p.b.-level ethanol could be applied to both the present breath-alcohol detectors and future unobtrusive alcohol sniffers that require ultrahigh sensitivity.

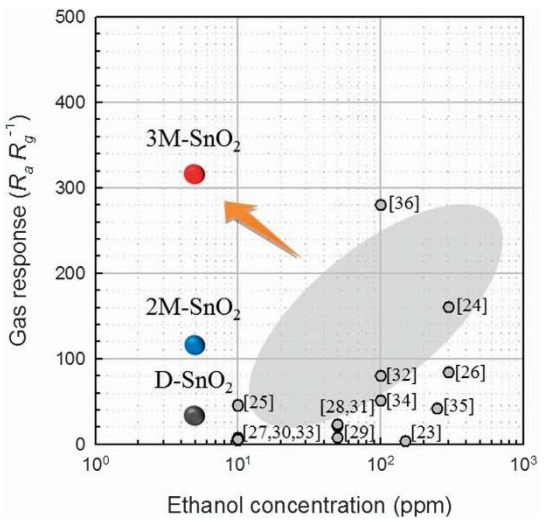

Figure 4 Gas response ($R_a R_g^{-1}$) of various SnO_2-based nanostructures and microstructures to ethanol, as reported in the literature[23–36] and the present study.

The one-pot spray pyrolysis method presented in this paper provides a straightforward and general synthetic route for the preparation of metal oxide spheres with well-defined and tunable multimodal pores. First, it is easy to prepare the various pure and multi-compositional metal oxide spheres via the atomization of droplets containing single or multiple metal precursors. In addition to the excellent control over the composition, the size of the spheres can be manipulated by changing the droplet size via the resonant frequency of the ultrasonic transducer. Second, the synergistic combination of the spherical and one-dimensional carbon-based templates provides precise control over the interconnectivity and multimodality of the pores. Efforts to enhance the macroporosity by introducing spherical templates have been reported,[41–43] but the nanoscale point contacts between the spherical pores often limits the mass transport through such pores, as evidenced by the present 2M-SnO_2-based sensor. The main breakthrough of the present study is the significantly enhanced interconnectivity between the different pore types, which was achieved by employing highly connecting, one-dimensional, carbon-based precursors, such as MWCNTs. The small mesopores (approximately 3 nm in size) and micropores (<2 nm in size) could be tuned by controlling the decomposition rate of the carbon-based precursors via the spray pyrolysis conditions or heating rate. The use of PS spheres with various sizes and MWCNTs with different diameters as templates will change the size of the macropores and mesopores, and the overall porosity can be controlled by changing the total concentration of carbon-based precursors. The application of various sizes of PS balls and/or MWCNTs can be used to achieve multimodal porosity. Finally, the interconnectivity between the different pore types can be enhanced by employing highly connecting, one-dimensional, carbon-based precursors, such as C nanofibers, as well as the MWCNTs used in this study. For example, we successfully prepared 3M-SnO_2 spheres with smaller and larger spherical macropores via the spray pyrolysis of a solution containing Sn-precursors, MWCNTs and PS balls with diameters of approximately 50 and 200 nm, respectively (Supplementary Figure S12). The scanning electron microscopic image clearly demonstrates the possible control over the size of the macropores. Knudsen diffusion depends on the molecular weight (or size) of the gas, and thus the size of the mesopores can be tuned to discriminate between gases with different sizes.[21,44] In addition, controlling the macropores, mesopores and micropores is extremely important for increasing or optimizing the accessibility of gases and ions to the surfaces of a material. From this perspective, the realization and tuning of multimodal pores with a high level of control over their size, distribution, volume and interconnectivity in the present study could provide a general solution for improving the performance of many

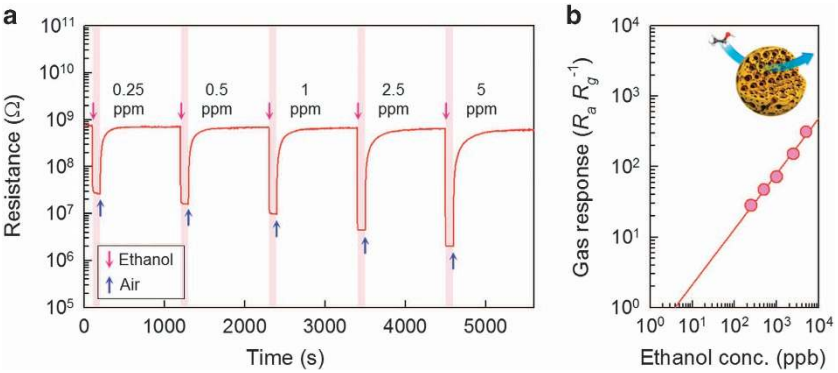

Figure 5 (**a**) Dynamic gas-sensing transients of the 3M-SnO_2 spheres to 0.25–5 p.p.m. of ethanol at 400 °C. (**b**) The gas responses (R_a R_g^{-1}) as a function of ethanol concentration under the same conditions.

energy and environmental applications, such as Li-ion batteries,[45] supercapacitors,[46] catalysts[47,48] and gas sensors.

CONCLUSIONS

The one-pot spray pyrolysis of droplets containing a metallic source, macroscale PS spheres and one-dimensional, mesoscale-diameter MWCNTs was developed as a facile synthetic route for the preparation of highly interconnected and tunable multimodal pores in SnO_2 spheres. The trimodal pores of the SnO_2 spheres (pore sizes ≈3, 20 and 100 nm) were prepared with spray pyrolysis and a subsequent heat treatment. An unprecedentedly high response to p.p.b. level of ethanol was accomplished by introducing additional large mesopores (approximately 20 nm in size) via one-dimensional MWCNT templates and was attributed to the increased pore-size-dependent Knudsen gas diffusion and enhanced gas accessibility through the highly connected one-dimensional pores. The precise control over, as well as the tuning of, multimodal pores in metal oxide nanostructures provides a new and general strategy for enhancing the performance of various energy and environmental applications.

CONFLICT OF INTEREST

The authors declare no conflict of interest.

ACKNOWLEDGEMENTS

This work was supported by a grant from the National Research Foundation of Korea (NRF), which was funded by the Korean government (Ministry of Education, Science, and Technology (MEST), Grant No. 2013R1A2A1A01006545).

1 Cui, C., Gan, L., Li, H.-H., Yu, S.-H., Heggen, M. & Strasser, P. Octahedral PtNi nanoparticle catalysts: exceptional oxygen reduction activity by tuning the alloy particle surface composition. *Nano Lett.* **12**, 5885–5889 (2012).
2 Poizot, P., Laruelle, S., Grugeon, S., Dupont, L. & Tarascon, J.-M. Nano-sized transition-metal oxides as negative-electrode materials for lithium-ion batteries. *Nature* **407**, 496–499 (2000).
3 Han, X., Jin, M., Xie, S., Kuang, Q., Jiang, Z., Jiang, Y., Xie, Z. & Zheng, L. Synthesis of tin dioxide octahedral nanoparticles with exposed high-energy {221} facets and enhanced gas-sensing properties. *Angew. Chem.* **121**, 9344–9347 (2009).
4 Peng, G., Tisch, U., Adams, O., Hakim, M., Shehada, N., Broza, Y. Y., Billan, S., Abdah-Bortnyak, R., Kuten, A. & Haick, H. Diagnosing lung cancer in exhaled breath using gold nanoparticles. *Nat. Nanotechnol.* **4**, 669–673 (2009).
5 Tiemann, M. Porous metal oxides as gas sensors. *Chem. Eur. J.* **13**, 8376–8388 (2007).
6 Wagner, T., Haffer, S., Weinberger, C., Klaus, D. & Tiemann, M. Mesoporous materials as gas sensors. *Chem. Soc. Rev.* **42**, 4036–4053 (2013).
7 Waitz, T., Wagner, T., Sauerwald, T., Kohl, C.-D. & Tiemann, M. Ordered mesoporous In_2O_3: synthesis by structure replication and application as a methane gas sensor. *Adv. Funct. Mater.* **19**, 653–661 (2009).
8 Rossinyol, E., Prim, A., Pellicer, E., Arbiol, J., Hernandez-Ramirez, F., Peiro, F., Cornet, A., Morante, J. R., Solovyov, L. A., Tian, B., Bo, T. & Zhao, D. Synthesis and characterization of chromium-doped mesoporous tungsten oxide for gas sensing applications. *Adv. Funct. Mater.* **17**, 1801–1806 (2007).
9 Liu, H., Du, X., Xing, X., Wang, G. & Qiao, S. Z. Highly ordered mesoporous Cr_2O_3 materials with enhanced performance for gas sensors and lithium ion batteries. *Chem. Commun.* **48**, 865–867 (2012).
10 Devi, G. S., Hyodo, T., Shimizu, Y. & Egashira, M. Synthesis of mesoporous TiO_2-based powders and their gas-sensing properties. *Sens. Actuators B* **87**, 122–129 (2002).
11 Hyodo, T., Nishida, N., Shimizu, Y. & Egashira, M. Preparation and gas-sensing properties of thermally stable mesoporous SnO_2. *Sens. Actuators B* **82**, 209–215 (2002).
12 Yang, P., Zhao, D., Margolese, D. I., Chmelka, B. F. & Stucky, G. D. Generalized synthesis of large-pore mesoporous metal oxides with semicrystalline frameworks. *Nature* **396**, 152–155 (1998).
13 Lee, J.-H. Gas sensors using hierarchical and hollow oxide nanostructures: overview. *Sens. Actuators B* **140**, 319–336 (2009).
14 Jing, Z. & Zhan, J. Fabrication and gas-sensing properties of porous ZnO nanoplates. *Adv. Mater.* **20**, 4547–4551 (2008).
15 Zhang, H., Zhu, Q., Zhang, Y., Wang, Y., Zhao, L. & Yu, B. One-pot synthesis and hierarchical assembly of hollow Cu_2O microspheres with nanocrystals-composed porous multishell and their gas-sensing properties. *Adv. Funct. Mater.* **17**, 2766–2771 (2007).
16 Kim, H.-R., Haensch, A., Kim, I.-D., Barsan, N., Weimar, U. & Lee, J.-H. The role of NiO doping in reducing the impact of humidity on the performance of SnO_2-based gas sensors: synthesis strategies, and phenomenological and spectroscopic studies. *Adv. Funct. Mater.* **21**, 4456–4463 (2011).
17 Kim, S.-J., Hwang, I.-S., Na, C. W., Kim, I.-D., Kang, Y. C. & Lee, J.-H. Ultrasensitive and selective C_2H_5OH sensors using Rh-loaded In_2O_3 hollow spheres. *J. Mater. Chem.* **21**, 18560–18567 (2011).
18 Lai, X., Li, J., Korgel, B. A., Dong, Z., Li, Z., Su, F., Du, J. & Wang, D. General synthesis and gas-sensing properties of multiple-shell metal oxide hollow microspheres. *Angew. Chem. Int. Ed.* **50**, 2738–2741 (2011).
19 Polleux, J., Gurlo, A., Barsan, N., Weimar, U., Antonietti, M. & Niederberger, M. Template-free synthesis and assembly of single-crystalline tungsten oxide nanowires and their gas-sensing properties. *Angew. Chem. Int. Ed.* **45**, 267–271 (2006).
20 Sakai, G., Matsunaga, N., Shimanoe, K. & Yamazoe, N. Theory of gas-diffusion controlled sensitivity for thin film semiconductor gas sensor. *Sens. Actuators B* **80**, 125–131 (2001).
21 Li, L.-L., Zhang, W.-M., Yuan, Q., Li, Z.-X., Fang, C.-J., Sun, L.-D., Wan, L.-J. & Yan, C.-H. Room temperature ionic liquids assisted green synthesis of nanocrystalline porous SnO_2 and their gas sensor behaviors. *Cryst. Growth Des.* **8**, 4165–4172 (2008).
22 Vuong, D. D., Sakai, G., Shimanoe, K. & Yamazoe, N. Preparation of grain size-controlled tin oxide sols by hydrothermal treatment for thin film sensor application. *Sens. Actuators B* **103**, 386–391 (2004).
23 Rella, R., Serra, A., Siciliano, P., Vasanelli, L., De, G., Licciulli, A. & Quirini, A. Tin oxide-based gas sensors prepared by the sol-gel process. *Sens. Actuators B* **44**, 462–467 (1997).
24 Mo, Y., Okawa, Y., Nakai, T., Tajima, M. & Natukawa, K. Preparation of SnO_2 films with high sensitivity and selectivity to C_2H_5OH by oxygen radical assisted electron beam evaporation for micro-machined gas sensors. *Thin Solid Films* **416**, 248–253 (2002).
25 Hellegouarc'h, F., Arefi-Khonsari, F., Planade, R. & Amouroux, J. PECVD prepared SnO_2 thin films for ethanol sensors. *Sens. Actuators B* **73**, 27–34 (2001).

26 Chen, Y. J., Nie, L., Xue, X. Y., Wang, Y. G. & Wang, T. H. Linear ethanol sensing of SnO_2 nanorods with extremely high sensitivity. *Appl. Phys. Lett.* **88**, 083105 (2006).
27 Zhang, Y., He, X., Li, J., Miao, Z. & Huang, F. Fabrication and ethanol-sensing properties of micro gas sensor based on electrospun SnO_2 nanofibers. *Sens. Actuators B* **132**, 67–73 (2008).
28 Ge, J.-P., Wang, J., Zhang, H.-X., Wang, X., Peng, Q. & Li, Y.-D. High ethanol sensitive SnO_2 microspheres. *Sens. Actuators B* **113**, 937–943 (2006).
29 Zhao, Q., Gao, Y., Bai, X., Wu, C. & Xie, Y. Facile synthesis of SnO_2 hollow nanospheres and applications in gas sensors and electrocatalysts. *Eur. J. Inorg. Chem.* 1643–1648 (2006).
30 Zhang, Y., Li, J., An, G. & He, X. Highly porous SnO_2 fibers by electrospinning and oxygen plasma etching and its ethanol-sensing properties. *Sens. Actuators B* **144**, 43–48 (2010).
31 Ying, Z., Wan, Q., Song, Z. T. & Feng, S. L. SnO_2 nanowhiskers and their ethanol sensing characteristics. *Nanotechnology* **15**, 1682–1684 (2004).
32 Huang, J., Yu, K., Gu, C., Zhai, M., Wu, Y., Yang, M. & Liu, J. Preparation of porous flower-shaped SnO_2 nanostructures and their gas-sensing property. *Sens. Actuators B* **147**, 467–474 (2010).
33 Chen, D., Xu, J., Xie, Z. & Shen, G. Nanowires assembled SnO_2 nanopolyhedrons with enhanced gas sensing properties. *ACS Appl. Mater. Interfaces* **3**, 2112–2117 (2011).
34 Yin, X. M., Li, C. C., Zhang, M., Hao, Q. Y., Liu, S., Li, Q. H., Chen, L. B. & Wang, T. H. SnO_2 monolayer porous hollow spheres as a gas sensor. *Nanotechnology* **20**, 455503 (2009).
35 Comini, E., Faglia, G., Sberveglieri, G., Pan, Z. & Wang, Z. L. Stable and highly sensitive gas sensors based on semiconducting oxide nanobelts. *Appl. Phys. Lett.* **81**, 1869–1871 (2002).
36 Liu, Y., Koep, E. & Liu, M. A highly sensitive and fast-responding SnO_2 sensor fabricated by combustion chemical vapor deposition. *Chem. Mater.* **17**, 3997–4000 (2005).
37 Li, K.-M., Li, Y.-J., Lu, M.-Y., Kuo, C.-I. & Chen, L.-J. Direct converstion of single-layer SnO nanoplates to multi-layer SnO_2 nanoplates with enhanced ethanol sensing properties. *Adv. Funct. Mater.* **19**, 2453–2456 (2009).
38 Kim, W. J., Lee, S. W. & Sohn, Y. Metallic Sn spheres and SnO_2@C core-shells by anaerobic and aerobic catalytic ethanol and co oxidation reactions over SnO_2 nanoparticles. *Sci. Rep.* **5**, 13448 (2015).
39 Tichenor, B. A. & Palazzolo, M. A. Destruction of volatile organic compounds via catalytic incineration. *Environ. Prog.* **6**, 172–176 (1987).
40 Driver Alcohol Detection System for Safety (DADSS) http://dadss.org accessed 14 June 2015.
41 Ko, Y. N., Park, S. B. & Kang, Y. C. Design and fabrication of new nanostructured SnO_2-carbon composite microspheres for fast and stable lithium storage performance. *Small* **10**, 3240–3245 (2014).
42 Skrabalak, S. E. & Suslick, K. S. Porous MoS_2 synthesized by ultrasonic spray pyrolysis. *J. Am. Chem. Soc.* **127**, 9990–9991 (2005).
43 Hyodo, T., Inoue, H., Motomura, H., Matsuo, K., Hashishin, T., Tamaki, J., Shimizu, Y. & Egashira, M. NO_2 sensing properties of macroporous In_2O_3-based powders fabricated by utilizing ultrasonic spray pyrolysis employing polymethylmethacrylate microspheres as a template. *Sens. Actuators B* **151**, 265–273 (2010).
44 Kida, T., Fujiyama, S., Suematsu, K., Yuasa, M. & Shimanoe, K. Pore and particle size control of gas sensing films using SnO_2 nanoparticles synthesized by seed-mediated growth: design of highly sensitive gas sensors. *J. Phys. Chem. C* **117**, 17574–17582 (2013).
45 Ren, Y., Ma, Z., Morris, R. E., Liu, Z., Jiao, F., Dai, S. & Bruce, P. G. A solid with a hierarchical tetramodal micro-meso-macro pore size distribution. *Nat. Commun.* **4**, 2015 (2013).
46 Yun, S., Kang, S.-O, Park, S. & Park, H. S. CO_2-activated, hierarchical trimodal porous graphene frameworks for ultrahigh and ultrafast capacitive behavior. *Nanoscale* **6**, 5296–5302 (2014).
47 Mitchell, S., Michels, N.-L., Kunze, K. & Perez-Ramirez, J. Visualization of hierarchically structured zeolite bodies from macro to nano length scales. *Nat. Chem.* **4**, 825–831 (2012).
48 Jong, K. P., Zecevic, J., Friedrich, H., Jongh, P. E., Bulut, M., Donk, S., Kenmogne, R., Finiels, A., Hulea, V. & Fajula, F. Zeolite Y crystals with trimodal porosity as ideal hydrocracking catalysts. *Angew. Chem. Int. Ed.* **49**, 10074–10078.

Supplementary Information accompanies the paper on the NPG Asia Materials website (http://www.nature.com/am)